Elastic properties of graphene flakes: boundary effects and lattice vibrations

S. Bera,[1,2] A. Arnold,[2] F. Evers,[1,2] R. Narayanan,[3] and P. Wölfle[1,2]

[1]*Institut für Theorie der Kondensierten Materie, Karlsruhe Institute of Technology, D-76128 Karlsruhe, Germany*
[2]*Institut für Nanotechnologie, Karlsruhe Institute of Technology, D-76021 Karlsruhe, Germany*
[3]*Department of Physics, Indian Institute of Technology Madras, Chennai-600036, India*
(Dated: March 24, 2010)

We present a calculation of the free energy, the surface free energy and the elastic constants ("Lamé parameters" i.e, Poisson ratio, Young's modulus) of graphene flakes on the level of the density functional theory employing different standard functionals. We observe that the Lamé parameters in small flakes can differ from the bulk values by 30% for hydrogenated zig-zag edges. The change results from the edge of the flake that compresses the interior. When including the vibrational zero point motion, we detect a decrease in the bending rigidity, κ, by $\sim 26\%$. This correction is depending on the flake size, N, because the vibrational frequencies flow with growing N due to the release of the edge induced compression. We calculate Grüneisen parameters and find good agreement with previous authors.

I. INTRODUCTION

Since its fabrication has become technologically feasible[1], graphene has been in the focus of frontier research[2–4]. One of its most celebrated properties are its massless low energy excitations[5,6] ("Dirac fermions"), which emanate from the symmetries of the honeycomb lattice. The electronic properties of graphene *flakes* are quite different from bulk graphene due to the finite size and the presence of edges[7,8]. In particular, calculations suggest that the zigzag edges of graphene nano-ribbons (quasi 1d) have two flat bands at the Fermi energy[9,10] that introduce magnetism[11–18]. Recent theoretical studies on zigzag edged graphene flakes also confirm a tendency towards edge magnetism[17–20]. This gives additional motivation for fabricating graphene based nano structures[21–26] for further studies. The fabrication of such structures with well defined edges still poses a considerable technological challenge. Therefore, only very few experiments with structures exhibiting zigzag edges have been reported[27–29]; a detailed investigation of the edge physics still needs to be done.

An increased interest in the *elastic* properties of graphene has developed recently[21,30–43]. This is, for instance, because experiments suggest that graphene samples exhibit a corrugated structure[28,44–46] ("ripples") even at relatively low temperatures. Their origin is thought to be due to residual elastic strain produced by the experimental preparation technique[47].

Also for elastic properties, edge effects can be highly relevant. For this reason, *flake* elastic properties are certainly interesting in their own right. Namely, there is an intimate relation between the electronic structure and the atomic geometry of graphene. For example, the electronic spectrum of a certain class of arm-chair graphene nano-ribbons is reported to acquire a spectral gap due to an edge induced lattice dimerization along the transport
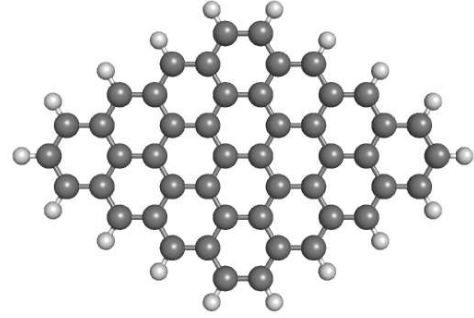

FIG. 1: Geometry of the $N \times N$ hydrogenated graphene flakes(here N=4), that we have used for the density functional calculations.

direction[13].

In our study we investigate the free energy, the elastic properties, and the phonon spectrum of $N \times N$ graphene sheets ("flakes") as displayed in Fig. 1 using the density functional theory (DFT). We show, that the different chemical nature of C-C bonds at the hydrogenated edge as compared to the bulk leads to an nearly homogenous compression, i.e. strain. As a consequence, the average C-C-distance in a 3×3 flake is reduced by a substantial amount, 0.3%; for comparison, strain as achieved in typical pressure experiments does not usually exceed values $\sim 1\%$[34,48,49].

The presence of the surface induced strain leaves various traces in the flakes' interior observables. (a) The flakes elastic constants, i.e. the Lamé parameters, are enhanced as compared to the bulk case. For isotropic strain in smallest flakes (3×3), the (inverse) compressibility $\mu + \lambda$ (precise definition see below, Eq. (2)) increases by 30%; for shear forces the increase is even bigger, almost a factor of 2. (b) Under bond compression the inter-

atomic forces typically increase, so that even the short wavelength vibrations, in particular the optical phonons, exhibit a "blue shift" of their frequencies with decreasing flake sizes. This flow can be seen in the variation of the Raman spectra with strain[27,48,50–53] and can be described in the standard manner by Grüneisen parameters. The values that we find here of Grüneisen parameters, agree reasonably well with previous reports[48,51,54].

Even though one might suspect, that our topics have already been dealt with extensively in the literature[53–57], a detailed investigation of the elastic properties of nanoflakes is yet to be done; this refers, in particular, to an analysis of edge and finite size effects of hydrogenated zig-zag flakes which we perform in this work.

II. FREE ENERGY OF HOMOGENOUS, PLANAR FLAKES

We consider the free energy of a graphene flake as depicted in Fig. 1 with a homogenous C-C-distance, d, as the sum of all its bond energies:

$$F_N(d) = N_{\rm i}\Psi(d) + N_{\rm e}\psi(d) + N_{\rm c}\psi^{\rm c}(d) + \frac{\phi^{\rm e}(d)}{N_{\rm e}} + \frac{\phi^{\rm i}(d)}{N_{\rm i}} \quad (1)$$

where $N_{\rm i}$ denotes the number of internal C-C-bonds with an associated binding energy Ψ, $N_{\rm e}$ denotes the number of edge located C-C-bonds with energy ψ and $\psi^{\rm c}$ includes the corner contributions, where $N_{\rm c}$ is the number of bonds linking the corner atoms, $N_{\rm c}$=6 in Fig. 1. The binding energy per C-C-CH edge group is close to 2ψ but not identical to it. For instance, ψ also includes corrections of internal bonds, that still "feel" the presence of the surface. Similarly, $N_c\psi^{\rm c}$ is approximating the binding energy of the corner groups (two HC-CH groups and two C-CH-C groups).

We mention, that the representation (1) is slightly simplified in the following sense. In general, the boundary (shape) of a given flake, e.g as depicted in Fig. 1, does not share the hexagonal symmetry of the honeycomb lattice. For this reason, in flakes with a fully relaxed atomic structure bond lengths and bond angles are not strictly all the same. Our DFT-calculations indicate, however, that such distortions, though clearly detectable, give only small corrections to those phenomenological parameters that we are mostly interested in.

The *continuum* theory of $2d$-membranes has been devised for an inhomogeneous flake with neighboring bonds exhibiting slowly (in space) varying bond distances, $d(\mathbf{r})$, and angles. In this formulation the elastic energy is represented by the functional[58],

$$E = \frac{\kappa}{2}\int_{\mathcal{A}} d^2\mathbf{r}(\nabla^2 h)^2 + \frac{\mu+\lambda}{2}\int_{\mathcal{A}} d^2\mathbf{r}\,(u_{xx}+u_{yy})^2$$
$$+\frac{\mu}{2}\int_{\mathcal{A}} d^2\mathbf{r}\,\left[4u_{xy}^2 + (u_{xx}-u_{yy})^2\right]. \quad (2)$$

The flake coordinates are given with respect to a planar reference state with area $\mathcal{A}$, that lives in the $\mathbf{r}$=(x,y)-plane; accordingly, the *in* plane coordinates constitute the displacement vector, $\mathbf{u}(x,y)$, that measures the translation of each membrane point (x,y,z) with respect to the reference state. The *out of* plane distortions define the height field $h(x,y)$; for the planar case h=0. $\mathbf{u}$ and h together constitute the strain tensor $(i,j=x,y)$,

$$u_{ij} = \frac{1}{2}\left[\partial_i u_j + \partial_j u_i + \partial_i h \partial_j h + \sum_k \partial_i u_k \partial_j u_k\right]. \quad (3)$$

It is clear that the form of u_{ij} depicted in Eq. (3) is symmetric construction, with respect to the spatial derivatives of $\mathbf{u}$ ensure its invariance under in plane rotations by 90° which correspond to $\mathbf{u} \propto (y,-x)$.

The total elastic energy (2) is a sum over contributions which resemble local oscillators in the membrane plane. The first term is proportionate to the curvature $\nabla^2 h$ and introduces the bending rigidity κ. It describes the energy cost for bending the membrane without changing the bond lengths or in plane bond angles.[76] The Lamé parameters, λ and μ, appearing in the second and third term of Eq. (2) describe the in plane rigidity.

For homogenous, planar membranes the elastic theory (2) may be considered as a continuum approximation to (1) which does not make explicit reference to boundary terms. Edges are accounted for only in the boundary conditions and (possibly) in a dependency of the Lamé parameters on the position with respect to the edge. Usually not included in (2) is the fact that this spatial dependency supports long range terms, $\sim 1/$flakesize. They modify the Lamé parameters appearing in (2) even inside the flake's interior.

Phenomenological parameters

Isotropic strain: In order to illustrate the cooperative effect between surface and bulk, we consider an expansion of (1) in terms of the variable ε=$(d - d_0)/d_0$; ε quantifies the strain inside the flake. The bulk free energy per bond has an expansion,

$$\Psi = \Psi_0 + \frac{1}{2}\Psi_2\,\varepsilon^2 + \frac{1}{6}\Psi_3\,\varepsilon^3 + \frac{1}{24}\Psi_4\,\varepsilon^4\ldots \quad (4)$$

where the bulk bond length d_0 is to be determined at $N_{\rm i,e} \to \infty$. The surface free energy may also be expanded about a minimum bond length, $d_0^{\rm e}$, but in general $d_0^{\rm e} \neq d_0$. After all, in the limit $N_{\rm i,e} \to \infty$, just the first term in Eq. (1) contributes to the free energy per area and therefore d_0 needs to minimizes Ψ, only. Hence, we introduce the relative deviation of surface and bulk optimal bond lengths, $\mathfrak{d}$=$(d_0 - d_0^{\rm e})/d_0$, so that we have an expansion

$$\psi = \bar\psi_0 + \frac{1}{2}\bar\psi_2\,(\varepsilon+\mathfrak{d})^2 + \frac{1}{6}\bar\psi_3\,(\varepsilon+\mathfrak{d})^3 + \frac{1}{24}\bar\psi_4\,(\varepsilon+\mathfrak{d})^4\ldots$$
$$\equiv \psi_0 + \psi_1\,\varepsilon + \frac{1}{2}\psi_2\,\varepsilon^2 + \frac{1}{6}\psi_3\,\varepsilon^3 + \ldots \quad (5)$$

where the coefficients in the second line are defined in terms of the expansion the line before. The elastic properties of the flake are determined by the expansion parameters $\Psi_{2,3,4}, \psi_{1,2,3}$.

At any finite value of $N_{\mathrm{i,e}}$, optimization must also include the boundary (i.e. surface) terms and therefore the optimal value of ε, ε_N, is non-vanishing in this case; specifically,

$$
\begin{aligned}
\varepsilon_N &= -\frac{\psi_1}{\Psi_2}\frac{N_{\mathrm{e}}}{N_{\mathrm{i}}} \\
&\approx -\mathfrak{d}\frac{\bar{\psi}_2}{\Psi_2}\frac{N_{\mathrm{e}}}{N_{\mathrm{i}}}.
\end{aligned} \tag{6}
$$

In order to calculate the feedback of this shift into the elastic parameters, we expand F in the vicinity of its minimum, ε_N, to the fourth order in ε. Recalling that this corresponds to a strain $\mathbf{u}(\mathbf{x})=\varepsilon\mathbf{x}$ we can compare the result with Eq. (2) and thus find:

$$
\begin{aligned}
\mu + \lambda &= \frac{1}{4}\left(\Psi_2 + \frac{N_{\mathrm{e}}}{N_{\mathrm{i}}}\psi_2\right) + \frac{1}{4}\Psi_3\varepsilon_N \\
&+ \frac{\varepsilon}{12}\left(\Psi_3 + \frac{N_{\mathrm{e}}}{N_{\mathrm{i}}}\psi_3 + \Psi_4\varepsilon_N\right).
\end{aligned} \tag{7}
$$

The first term in the rhs-expression (7) simply accounts for the separate, additive contributions of bulk and surface (i.e. edge) free energies. The edge contribution, that appears here, could formally be accounted for in a generalized version of Eq. (2) where one adds a boundary term. Similarly, by allowing for a dependency of the Lamé parameters on strain itself, one could also include additive an-harmonic effects, second bracket first two terms. In either case, the phenomenological parameters are universal in the sense, that they are the same for each flake size and geometry.

The interesting pieces are the terms in ε_N, which are mixing surface and bulk parameters: $\Psi_3\varepsilon_N \sim \psi_1\Psi_3/\Psi_2$. They encode the "cooperative" effect between boundary induced strain and bulk anharmonicities. It is due to them, that the flakes elastic parameters need to be adjusted in principle for every geometry separately.

Shear strain: An analogous analysis as for the isotropic strain also applies to shear forces. The expansion is even in the shear strain $\mathbf{u} = (0, \varepsilon_{\mathrm{s}}x)$:

$$
\Psi = \Psi_0 + \frac{1}{2}\tilde{\Psi}_2\,\varepsilon_{\mathrm{s}}^2 + \frac{1}{24}\tilde{\Psi}_4\,\varepsilon_{\mathrm{s}}^4 + \dots \tag{8}
$$

$$
\psi = \psi_0 + \frac{1}{2}\tilde{\psi}_2\,\varepsilon_{\mathrm{s}}^2 + \frac{1}{24}\tilde{\psi}_4\,\varepsilon_{\mathrm{s}}^4 + \dots. \tag{9}
$$

The new expansion parameters, $\tilde{\Psi}_i, \tilde{\psi}_i, i = 2, 4, \dots$, are, in general, dependent on the flake geometry. Again, by comparing to Eq. (2) we find

$$
\mu = \tilde{\Psi}_2 + \tilde{\psi}_2 + \frac{1}{12}\varepsilon_{\mathrm{s}}^2\left(\tilde{\Psi}_4 + \tilde{\psi}_4\right). \tag{10}
$$

Here, surface and bulk free energies give strictly additive contributions, and a cooperative effect does not emerge.

III. DENSITY FUNCTIONAL CALCULATIONS

A. Method

In Fig. 1 we display the geometry of the $N \times N$-graphene flake that is employed in our calculations: $N_{\mathrm{i}} = (N-1)(3N-1)$, $N_{\mathrm{e}} = 8(N-1)$. Electronic structure calculations have been performed for a given atomic configuration (C-C distance, flake geometry etc.) on the basis of the density functional theory as implemented in the quantum chemistry package TURBOMOLE[59]. We are comparing GGA functionals (BP86[60,61], PBE[62,63]) with a hybrid functional (B3LYP[64]) and use a minimal basis set (SVP[65]). Specifically, we are working at zero temperature and approximate the free (i. e. ground state) energy, Eq. (1), by the DFT estimate for the total binding energy of the flake:

$$
F_{\mathrm{el}}(N, d) := E_{\mathrm{el}}(N, d) - E_{\mathrm{free}}(N). \tag{11}
$$

with,

$$
E_{\mathrm{free}}(N) = N_{\mathrm{H}}E_{\mathrm{H}} + N_{\mathrm{C}}E_{\mathrm{C}} \tag{12}
$$

where $E_{\mathrm{H/C}}$ denote the DFT energies of a free charge neutral hydrogen/carbon atom and $N_{\mathrm{H/C}}$ denotes the number of hydrogen/carbon atoms in the flake.

B. Results and Discussion

Isotropic strain: A sequence of DFT calculations has been performed for $N=3\dots 9$ and different values of the C-C distance, d. For each distance, $F_{\mathrm{el}}(N, d)$ has been calculated. In order to extract the expansion coefficients of Eq. (1), $\Psi(d), \psi(d), \psi^{\mathrm{c}}(d), \phi^{\mathrm{e}}(d), \phi^{\mathrm{i}}(d)$, we have performed five parameter fits on sets of raw DFT data. These fits were applied to three data sets consisting of $\{N\}=3,\dots 7$, $\{N\}=3\dots 8$ and $\{N\}=3\dots 9$. The results for the surface, bulk and corner free energy have been displayed in Fig. 2. The scatter between the fitting parameters belonging to different data sets is relatively small, which illustrates the stability of the fit.

The lattice constant of bulk graphene is estimated from the minimum position of $\Psi(d)$ Fig. 2, upper panel as $d_0=2.706a_0$, where $a_0=0.529\mathring{A}$ denotes the Bohr radius. Comparing this position to the minimum of the edge (surface) free energy, Fig. 2, center panel, $d_0^{\mathrm{e}}=2.694a_0$, we find $\mathfrak{d}=0.44\%$. This indicates clearly the compression of the C-C bond length near the edge. The shift of the minimum position to lower values becomes even more pronounced near the corners, i.e. in $\psi^{\mathrm{c}}(d)$, see Fig. 2, lower panel.

Furthermore, we can perform a certain consistency check by evaluating the bond energies. We have a binding energy $\Psi(d_0)=-5.22\mathrm{eV}$ for bulk carbon atoms. The binding energy of H-atoms near edges (C-C-CH group) is approximately $\Delta E_{\mathrm{H}}^{\mathrm{e}}\approx 2\psi(d_0)-2\Psi(d_0)\approx -4.6\mathrm{eV}$; when going to the corners (HC-CH and C-CH-C groups) we
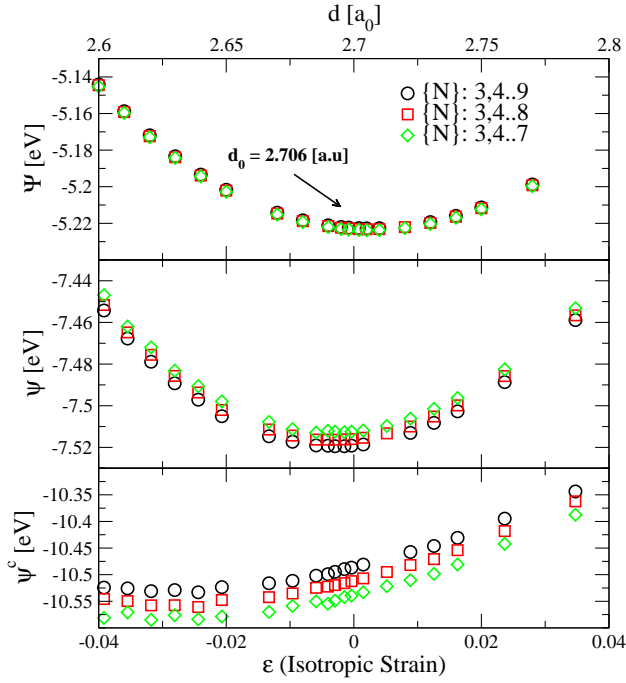
FIG. 2: Bulk (Ψ), surface (edge, ψ) and corner ($\psi^{\rm c}$) free energy per carbon bond in the graphene flakes, Fig. 1, calculated with density functional theory (BP86-functional). Data based on the evaluation of three sets of flake sizes ranging from $\{N\}=3\ldots9$, and a 5 parameter fit to Eqs. (1,11) per d values. ($a_0:=0.529$ $\mathring{A}$.)

	$d_0[\mathring{A}]$	$d_0^{\rm e}[\mathring{A}]$
BP86	$1.432^{\pm0.002}$	$1.427^{\pm0.001}$
B3LYP	$1.426^{\pm0.001}$	$1.421^{\pm0.002}$
PBE	$1.431^{\pm0.001}$	$1.426^{\pm0.005}$

TABLE I: Minimum C-C bond length as extracted from bulk free energy and surface free energy correspondingly (see Fig. 2, upper and middle panel). The distance in d_0 and $d_o^{\rm e}$ leads to a nearly homogenous pressure on the flake that modifies elastic and electronic-structure properties. Data is shown for three different functional used in DFT calculation.

have $\Delta E_{\rm H}^{\rm c}\approx\psi^{\rm c}(d_0)-\Psi(d_0)\approx-5.3$ which is roughly consistent with $\Delta E_{\rm H}^{\rm e}$, as it should be.

To obtain also the other phenomenological parameters, a second (polynomial) fit of the traces $\Psi(d),\psi(d)$, Fig. 2, according to Eqs. (4,5) has been performed; all fitting parameters are summarized in Tab. I,II and III.

When fitting the raw data to get $\Psi,\psi,\psi^{\rm c}$ the terms in $1/N_{\rm i,e}$ could not be neglected for the system sizes, that we considered. The corresponding amplitudes are displayed in Fig. 3. Unlike it was the case with the previous data, Fig. 2, the amplitudes $\phi^{\rm i,e}$ of the $1/N_{\rm i,e}$-corrections still exhibit a considerable variation with increasing system size, which is probably due to even higher order terms that have been neglected in the expansion Eq. (1). Interestingly, while the magnitude of $\phi^{\rm i,e}(\varepsilon)$ is still shifting

	$-\Psi_0$ [eV]	$\frac{1}{2}\Psi_2$ [eV]	$-\frac{1}{6}\Psi_3$ [eV]
BP86	$5.223^{\pm0.001}$	$46.301^{\pm0.082}$	$128.301^{\pm1.915}$
B3LYP	$5.008^{\pm0.001}$	$47.723^{\pm0.362}$	$154.59^{\pm31.446}$
PBE	$5.373^{\pm0.004}$	$45.57^{\pm0.43}$	$187.309^{\pm24.448}$

TABLE II: Bulk free energy coefficients as defined in Eq. (4). These coefficients are extracted from fitting Eq. (4) to the data in Fig. 2, upper panel.

	$-\psi_0$ [eV]	ψ_1 [eV]	$\frac{1}{2}\psi_2$ [eV]	$-\frac{1}{6}\psi_3$ [eV]
BP86	$7.515^{\pm0.006}$	$0.285^{\pm0.015}$	$44.93^{\pm0.43}$	$112.745^{\pm18.718}$
B3LYP	$7.187^{\pm0.006}$	$0.261^{\pm0.015}$	$45.586^{\pm2.154}$	—
PBE	$7.63^{\pm0.01}$	$0.308^{\pm0.011}$	$47.503^{\pm1.082}$	—

TABLE III: Edge (surface) coefficients as defined in Eq. (5). These coefficients are extracted from fitting Eq. (5) to the data in Fig. 2, middle panel.

the slope and perhaps also the sign of the two functions has converged, already. Under this assumption we may conclude, that both amplitudes flow closer to zero values when ε increases. This behavior is compatible with the simple expectation, that the main effect incorporated in the $1/N_{\rm i,e}$-corrections is the discreteness of the flake's electronic spectrum with level spacings $\Delta_{\rm i,e}$ for bulk and surface modes. With increasing ε the bandwidth decreases and so do $\Delta_{\rm i,e}$ and $\phi^{\rm i,e}$.

Shear strain: A largely analogous method as was adopted for the isotropic strain, has also been applied for shear forces. In this case, the convergence of the DFT calculations turned out to be considerably more difficult, so that the investigated system sizes range from $\{N\}=3\ldots7$, only. From our fitting procedure we could determine the response of the bulk and surface energy to
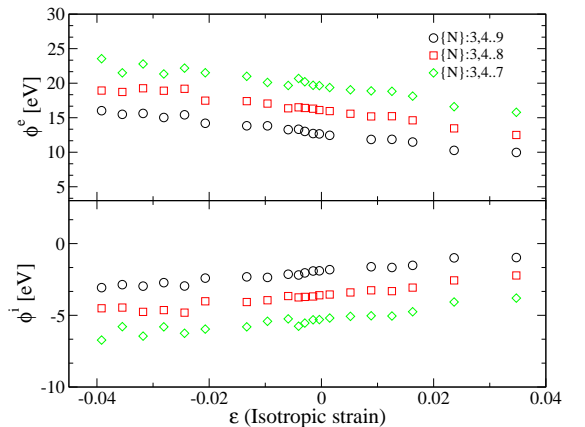

FIG. 3: Dependency of the amplitudes $\phi^{\rm i,e}$ describing the corrections in $1/N_{\rm e,i}$ to the binding energy $\Delta F_{\rm el}(N)$. Data were obtained by the 5 parameters fit, already underlying the traces shown in Fig. 2.
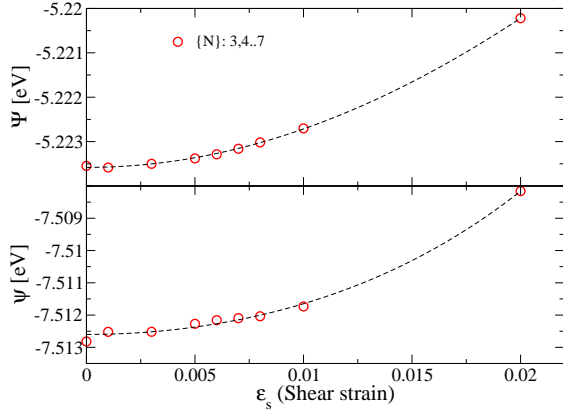
FIG. 4: Change in the free energy when applying a shear strain in graphene flakes. Upper panel shows the change in bulk free energy per interior C-C bond; lower panel exhibits change in surface (edge) free energy per C-C bond. Data sets are for system sizes {N}=3...7 and extracted from an expression analogous for shear to Eqs. (1,11). The lines indicate the polynomial fit according to Eqs. (8,9) with parameter given in Tab. IV.

[eV]	$\frac{1}{2}\tilde{\Psi}_2$	$-\frac{1}{24}\tilde{\Psi}_4$	$\frac{1}{2}\tilde{\psi}_2$	$\frac{1}{24}\tilde{\psi}_4$
BP86	$8.396^{\pm 0.426}$	$871^{\pm 50\%}$	$8.99^{\pm 3.29}$	$5237^{\pm 60\%}$

TABLE IV: Bulk and surface shear free energy coefficients as extracted from fitting Eq. (8) (Eq. (9)) to the data in Fig. 4 upper panel (lower panel).

the shear strain, ε_s, as shown in Fig. 4. The parameters entering Eqs. (8,9) can be extracted and are listed in Tab. IV.

IV. FLAKE ELASTIC PROPERTIES

In the previous subsection, the focus was on the behavior of the free energy on the flake size under isotropic and shear strain. In this section, we discuss and illustrate what our previous findings imply for the elastic properties of a single flake with a fixed size, N. Partly, we are considering the same set of data again, but now plotting observables directly for N fixed.

1. Homogenous isotropic strain

Fig. 5 shows, how the excess energy per unit cell grows under increasing strain for different flake sizes N. It is readily seen from this plot, that there is a shift of the equilibrium lattice constant $d(N)$ to smaller values. In the light of the previous section, this shift is the expected consequence of the surface induced strain ε_N. The inset shows, the scaling with N_e/N_i.

In addition, we also extract the flake elastic constant $\mu+\lambda$ from the parabolic shape of the curves, Fig. 5. To
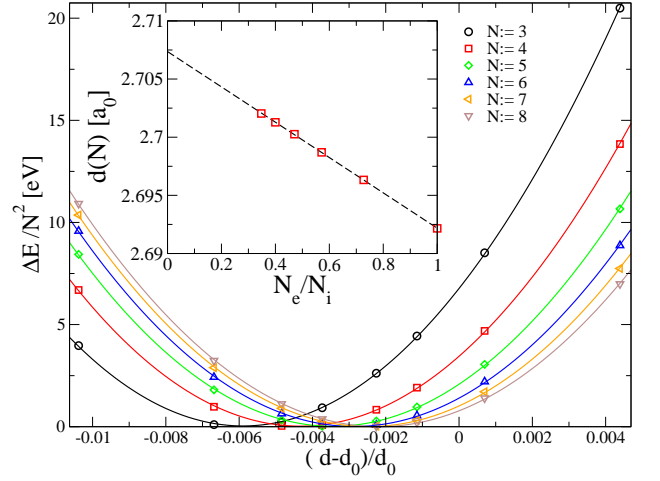

FIG. 5: Excess energy ΔE per unit cell generated by rescaling all bond length, d, (homogeneous, isotropic strain). ΔE exhibits flow of the equilibrium bond length with the linear flake size N. Main panel: ΔE over bond length d employed in the simulation. d is measured relative to the bulk bond length. The lines serve as a guide to the eyes. Inset: Extrapolating the equilibrium bond length $d(N)$ into the bulk limit: $d_0 = 2.707 \pm 0.001$.

this end, we replot the data in Fig. 6 left, so as to highlight the curvature and its strain dependency. On the basis of Eq. (7) we can conclude, that the offset of the curves is a consequence of (a) the presence of the surface and the extra energy required for its compression (term N_e/N_i in Eq. (7)) and (b) the feedback of the surface strain ε_N into the bulk C-C distance. Extrapolating the zero strain values into the limit, $N\to\infty$, we recover the previously derived bulk limit value. This check is displayed in Fig. 6, right. The plot also reveals, that the deviation of elastic parameters from their bulk values in small flakes may not be very small. For our smallest flakes, $N=3$ it reaches almost 30%.

Additional information can be extracted from Fig. 6 left, about anharmonicities which manifest themselves in the slope of the curves displayed. This pre-factor of the an-harmonic term (linear in ε) in Eq. (7) admits the following interpretation. The slope changes with increasing N since the contributions of the surface (ψ_3-term) and the surface induced bulk compression ($\Psi_4\varepsilon_N$-term) diminish. A non-vanishing value of $\Psi_3/12$ for the slope will remain however even in the bulk limit.

2. Shear strain

Following the same strategy as we did before with Fig. 6, we plot in Fig. 7 the excess energy ΔE_s induced by pure shear strain, $\mathbf{u}(\mathbf{x}) = \varepsilon_s(0, x)$. Again, the plot emphasizes the curvature in this quantity, μ, and how it evolves with the flake size. Since ΔE_s is even in the
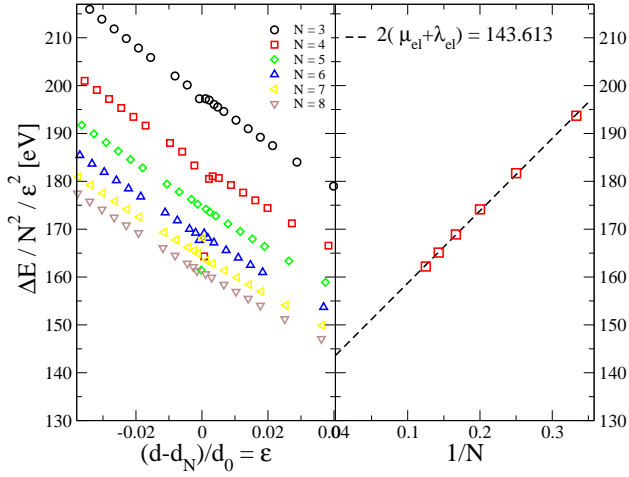
FIG. 6: Estimating the sum of the Lamé parameters $\mu_{el} + \lambda_{el}$ and the boundary correction (offset of traces) from ΔE displayed in the previous Fig. 5. Left: Data for curvature exhibit a slope which indicates the linear dependency of the Lamé parameter λ_{el} on strain. (Linear terms in μ_{el} do not appear, see Fig. 9.) Right: extrapolating the curvature at $\varepsilon = 0$ into the bulk limit.
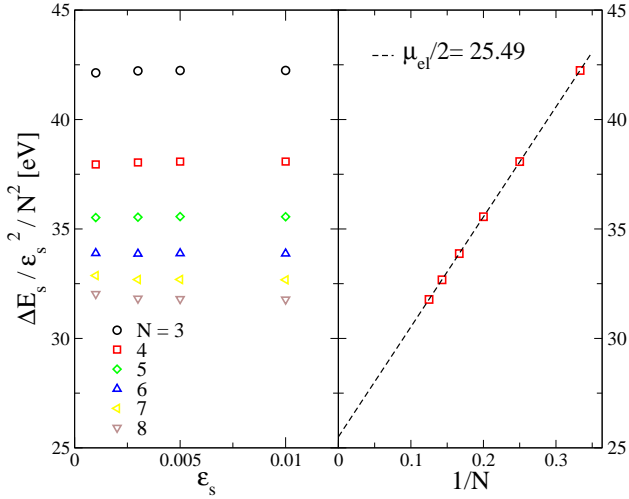

FIG. 7: Estimate for Lamé parameter μ_{el} determined from the excess energy ΔE_s per unit cell under pure shear strain with strength ε_s. (Procedure similar to previous Fig. 6.) Left panel: dependency of curvature of $\Delta E_s(\varepsilon_s)$ on the linear flake size N. Due to mirror symmetries of the unit cell, linear corrections do not appear for the shear parameter μ_{el}. Right: extrapolating the curvature into the bulk limit.

shear strain, only positive values of ε_s are given. Also, for the same reason an-harmonic terms exist only in the quartic order, so that the displayed data traces have zero slope. Similar to the previous case of isotropic strain, we also witness here a very strong dependency of the elastic constant on the flake size. In fact, for shear strain it reaches almost 70% for the small system sizes that we

	$d_0[\mathring{A}]$	$\mu_{el}+\lambda_{el}[eV]$	$\mu_{el}[eV]$	ν	$Y[N/m]$
BP86	$1.432^{\pm0.001}$	$70.715^{\pm0.011}$	$50.95^{\pm0.01}$	0.162	356.23
B3LYP	$1.427^{\pm0.001}$	$71.21^{\pm0.12}$	-	-	-
PBE	$1.431^{\pm0.002}$	$69.027^{\pm0.012}$	-	-	-
prev. calc.	1.42[37,66] 1.41[43] 1.45[68]	66.571[37]	49.45[37]	0.149[67], 0.173[31] 0.16[68] 0.31[39]	346[37] 307[41] 345[67] 336[68] 312[39]
expt. (Graphene)	-	-	-	-	342[34]
expt. (Graphite)	1.421[69] 1.422[71]	-	-	0.165[70]	371[71][a]

[a]assuming graphene thickness 0.335 nm.

TABLE V: Comparison of C-C-bond distance in bulk graphene, elastic constants , Poisson ratio(ν) and Young's modulus(Y) as extracted from Fig. (5,6,7) respectively by extrapolating the values in bulk limit ($N \to \infty$) with previous works. Data is shown for three different functionals we used in DFT calculation.

are considering.

3. Buckling induced strain

We present results from an additional DFT study, where we investigate the transverse stiffness of the graphene flake that gives rise to the elastic parameter κ. To this end we employ the following strategy. Each flake has a center pair or center ring of carbon atoms, see Figs. (1,8). To create a transverse probing field $h(\mathbf{r})$, we lift the center atoms by the distance h_0 over the reference plane. After this, the atomic structure of the flake is relaxed under the constraint, that the set of *edge atoms* (H-atoms and edge C-atoms) can move only within the reference plane; edge atoms cannot shift in h-direction.[77] In this way, a flake is equipped with a single ripple while at the same time the associated strain field $\mathbf{u}(\mathbf{x})$ remains negligibly small. In order to estimate the integrated curvature we numerically compute the bi-variate function which interpolates the scattered data values($h(\mathbf{r})$-field) at any predefined smooth mesh. We then use this interpolated function to perform the second order numerical derivative at any arbitrary precision.

Fig. 9 displays how the excess energy ΔE_h associated with the ripple grows with the increased integrated curvature,

$$I_\kappa = \frac{1}{2} \int d^2\mathbf{r} \ (\Delta h(\mathbf{r}))^2 \qquad (13)$$

The increase is linear, as expected from Eq. (2) with a slope that is only weakly dependent on the flake size, see inset Fig. 9, this implies that nonlinearities remain small as long as the ratio of the ripples amplitude and wave length , h_0/L, does not exceed $\sim 5\%$. The bending rigidity thus found is $\kappa_{el} = 1.24$ eV which is well consis-
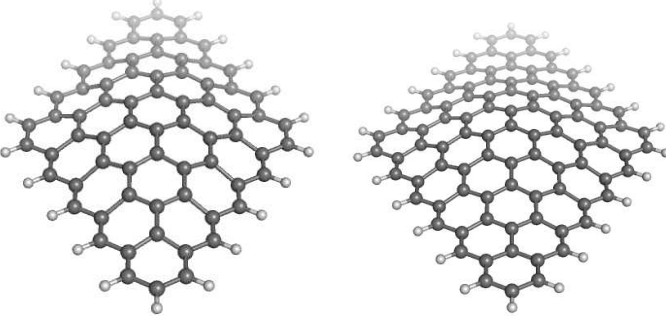
FIG. 8: Buckling flakes of N=5, 6 with different central configurations of carbon atoms. The atomic configuration of C atoms is relaxed under the constraint that the center atoms remain at a given height h_0 above the ground plane, while edge atoms (H and C) remain sitting within this plane ($h = 0$).

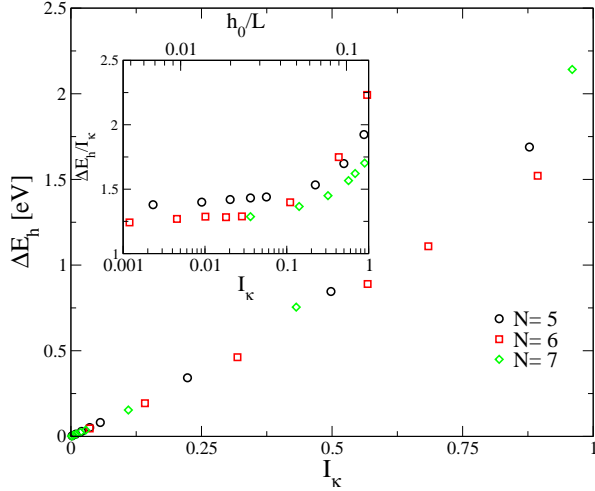tent with the value 1.1eV obtained by Fasolino, Los and Katsnelson[30].

FIG. 9: Estimating the Lamé parameter κ determined from the excess energy ΔE of a bulging flake with maximum height at h_0 over the unperturbed (flat) plane (see Fig. 8). Main panel: Change of energy ΔE with the integrated curvature $I_\kappa = \int d^2\mathbf{r} (\Delta h(\mathbf{r}))^2$ for different flake sizes N. Inset: The ratio $\kappa = \Delta E/I_\kappa$ depend on N due to the effect of edge compression.

Notice, that there is a significant scattering of almost 20% in earlier theoretical estimates for κ and derived quantities, see Tab. 2 in Ref. 72. Discrepancies appear because different theoretical techniques are being employed, e.g. empirical potentials[42] and density functional theory, but also because of modeling artefacts. For example, extracting κ from the elastic energy of carbon nano-tubes (radius R) requires a very careful extrapolation in $1/R$. If sub-leading terms are ignored, there is a pronounced tendency to overestimation, e.g. $\kappa = 1.46$ eV in Ref. 67. These authors used nano-tubes with smaller tube radius, hence bigger curvature, where nonlinear effects become important. We can check the bending rigidity using the same curvature in Fig. 9 (inset) as reported in Ref. 67 and find a reasonable agreement with their value.

V. ZERO POINT MOTION

In this chapter we extend our analysis of flake elastic properties and take also the zero point motion of the atom cores into account, that constitute the hexagonal lattice. Now, the free energy acquires a second term,

$$F(N,d) = F_{\text{el}}(N,d) + F_{\text{vib}}(N,d) \qquad (14)$$

with

$$F_{\text{vib}} = \frac{1}{2} \sum_p \hbar \omega_p(N,d) \qquad (15)$$

where p labels all the flake's vibrational modes. The vibrational excess energy associated with stretching the flake reads

$$\Delta F_{\text{vib}} = \frac{\hbar}{2} \sum_p \omega_p(N,d) - \omega_p(N,d(N)) \qquad (16)$$

where $\omega(N,d(N))$ denotes the vibration energies in the absence of strain and $d(N)$ the equilibrium bond length, see inset Fig. 5. Also ΔF_{vib} can be expanded in terms of the slow elastic modes,

$$\Delta F_{\text{vib}}[h,\mathbf{u}] = \frac{1}{2} \int_{\mathcal{A}} d^2\mathbf{r}\, \gamma_h \left(\Delta h(\mathbf{r})\right)^2 - \int_{\mathcal{A}} d^2\mathbf{r} \sum_{ij} \gamma_u^{ij} u_{ij}(\mathbf{r}), \qquad (17)$$

with expansion parameters γ_h, γ_u that represent averages of Grüneisen parameters over all vibrational modes. In a two-dimensional sample[78] with a mirror symmetry one expects $\gamma_u^{xy} = \gamma_u^{yx} = 0$; the change in phonon frequencies should be even in the shear strain, ε_s. Combining Eq. (17) with an expansion of ΔF_{el} in full analogy with Eq. (2) and after completing the square, we find,

$$\Delta F_{\text{el vib}}(N,d) = \frac{\kappa_{\text{el}} + \gamma_h}{2} \int_A d^2\mathbf{r}(\nabla^2 h)^2 + \frac{\mu_{\text{el}} + \lambda_{\text{el}}}{2} \int_A d^2\mathbf{r} \left(u_{ii} - \frac{\gamma_u^{ii}}{\mu_{\text{el}} + \lambda_{\text{el}}} \right)^2 + \frac{\mu_{\text{el}}}{2} \int_A d^2\mathbf{r} \left(u_{xx} - u_{yy} \right)^2 + u_{xy}^2. \qquad (18)$$
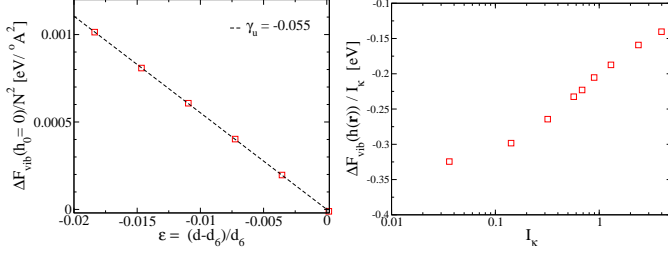
FIG. 10: Left: Dependency of ΔF_{vib} on isotropic strain for system size N=6. The slope defines γ_u as in Eq. (17). Right: Dependency of ΔF_{vib} on integrated curvature, $I_\kappa = \int d^2\mathbf{r} \ (\Delta h(\mathbf{r}))^2$, as in Fig. 9.

	BP86, N=6	prev. calc.	expt.
γ_u [eV/$\mathring{A}^2$]	-0.055	-	-
γ_h [eV]	-0.32	-	-
$\gamma_u/(\mu_{el} + \lambda_{el})$	-0.004	-	-
γ_D [eV/$\mathring{A}^2$]	2.6	2.7[66]	
γ_G [eV/$\mathring{A}^2$]	2.2	2.0[75]	1.99[48,52]

TABLE VI: Survey over the fitted Grüneisen parameters extracted from the data Fig. 10 and Fig. 11 respectively.

For clarity, we have indicated in this expression the bare electronic coefficients (i.e. with frozen atomic cores) by $\kappa_{el}, \mu_{el}, \lambda_{el}$. Likewise, the displacement field $\mathbf{u}(\mathbf{x})$ is defined with respect to the optimum flake geometry ignoring vibrational terms.

In this way we can observe two facts. (i) Vibrations modify the bare transverse stiffness κ_{el} in Eq. (18), $\kappa = \kappa_{el} + \gamma_h$. (ii) Vibrations also affect interatomic distances. The effect can be understood as an effective strain, which stretches the bare C-C distances: $\gamma_u^{ii}/(\mu_{el} + \lambda_{el})$. (iii) The change in the C-C bond lengths eventually feeds back into all elastic coefficients. Therefore, in a more complete treatment of higher order terms also modifications in μ_{el}, λ_{el} would occur.

A. DFT calculations of the Grüneisen parameters

In order to estimate the Grüneisen parameters, γ_h, γ_u, we should calculate the vibrational spectrum of flakes with and without applied strain. To this end we adopt the following procedure. For every flake size, N, we find the atomic geometry with the optimal electronic energy, see e.g. Fig. 1. This constitutes the set of freely relaxed "parent states". The relaxation ensures the Hessian, that characterizes interatomic forces, to become a positive definite matrix.[79]

In the present study we focus on the impact of phonons on the bulk elastic constants. There we may eliminate contributions of surface vibrations by assigning an infinite mass to the surface H and C atoms. Other than this, the calculation of vibrational modes and frequencies for the relaxed flake is a standard procedure[73,74].

Thereafter, each parent state thus obtained is used in order to create two new families. The first family is constructed to obtain γ_u. It derives by changing the bond length of edge C-C-pairs by a factor of $1 + \varepsilon$ keeping all atoms still inside the base plane (h=0). For each value ε the internal C-atoms are relaxed and the vibrational spectrum together with the average strain field, $I_u(\varepsilon) = \int d\mathbf{r}(u_{xx} + u_{yy})$, are recalculated. In this process it is important to have edge atoms at infinite mass.

This ensures that the flake energy is in a (constrained) minimum so that all frequencies are real.

In order to determine γ_h a second family has been constructed. It consists of the buckled flakes, Fig. 8, that we have studied in the previous section in order to extract κ_{el}. Again, after assigning infinite mass to the edge atoms for each family member, the vibrational spectrum and the consecutive modification of the zero point energy can be calculated.

B. Results and Discussion

In Figs. 10 the change in the zero point energy, ΔF_{vib}, is plotted over the integrated strain fields. The Grüneisen parameters are given by the slope near zero strain; their numerical values are listed in Tab. VI. For a discussion of our results we first recall, that the vibrational spectral density of states of the carbon sheet has a strong peak in the optical frequency regime, c.f. Fig. 11, near 1600 cm^{-1}. It is the "G-peak", that corresponds to an in-plane mode, where neighboring atoms vibrate in opposite direction as depicted in Fig. 12 (right). This mode gives the dominating contribution to the total zero point energy. Another significant contribution comes from the frequency range $500-1000$ cm^{-1}, where one observes the mixing of out-of-plane modes with in-plane modes. A third important mode is the "D-peak" near 1350 cm^{-1}, that reflects the breathing mode as shown in Fig. 12 (left). This mode is particularly interesting when studying finite size(edge) effects in graphene flakes. The reason is that, in bulk graphene the coupling of the D-peak to the electromagnetic fields is suppressed, since the D_{6h}-symmetry of the hexagonal unit cell remains intact and inhibits the formation of the dipole moment. By contrast, in flake with an overall symmetry that is lower than D_{6h}, the D-peak is observable with a strength proportional to the inverse flake size.

Therefore, we can understand the sign of γ_h as a consequence of a softening of these modes in the sample regions with non-zero curvature $(\Delta h(\mathbf{r}))^2$. Similarly, γ_u is negative, indicating the increase of the atomic oscillator frequency that occurs when the interatomic distance is diminished.

While the sign of $\gamma_{h,u}$ was not unexpected, it is noteworthy that the vibrational contributions to the phenomenological material parameters are actually not so
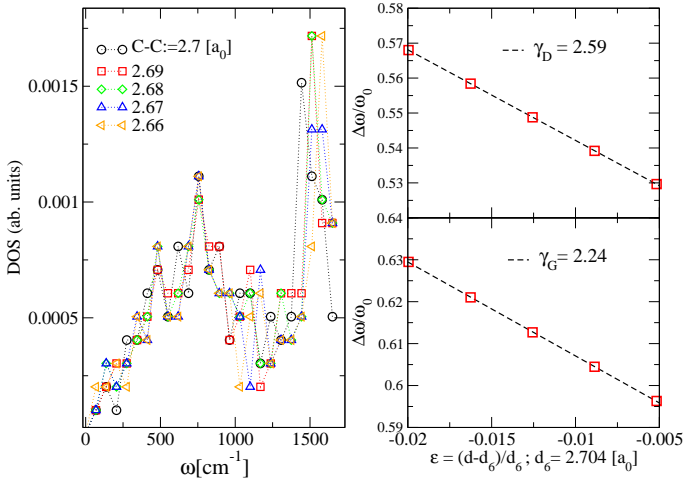
FIG. 11: Left panel: Phonon density of states for the flake of size N=6. Data sets are shown for different C-C bond distances. Upper right panel shows the flow of D-peak with in-plane strain. Lower right panel shows the variation of Raman G-peak with strain, where ω_0 is the Raman band frequency(≈ 2680 cm^{-1})[51]. The corresponding vibration modes are shown in Fig. 12.

small. The bare electronic bending rigidity, $\kappa_{\rm el}$ is reduced by as much as 26% down to $\kappa=\kappa_{\rm el} + \gamma_h$=0.88eV. Similarly, when expressing the effect of vibrations on the atomic lattice as an effective strain pushing the atoms to larger distances, then this strain reaches values up to 0.4%.

Here, we also calculate the Grüneisen parameters associated with individual modes (see Fig. 12). The right panel in Fig. 11 shows the flow of the Raman frequencies (upper half D, lower G) with the applied strain. The frequency decreases linearly (as described in Eq. (17)) with decreasing compression due to anharmonicity of the interatomic potential. The slope essentially estimates the Grüneisen parameters, $\gamma_{\rm G}$ and $\gamma_{\rm D}$ for the vibrations shown in Fig. 12. Our results for $\gamma_{\rm G}$, $\gamma_{\rm D}$ are consistent with the earlier experiments and first principal calculations (see Tab. VI) available in literature[48,52,66,75].
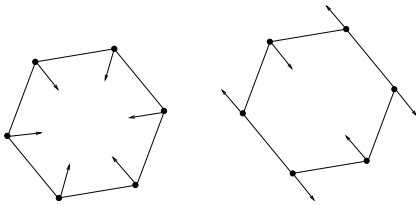

FIG. 12: Schematic diagram of vibrating modes that give rise to D(left) and G(right) peaks in Raman spectra of graphene.

VI. CONCLUSION

The elastic properties of edge hydrogenated graphene flakes have been investigated employing the density functional theory (DFT). Our study emphasizes the interplay between the edge and bulk properties which are mediated via long range elastic forces.

Specifically, we are able to disentangle bulk, surface and corner contributions to the free energy together with the leading higher order corrections. The binding energy per surface (edge) bond (7.5eV) is roughly two eV higher than the one for interior (bulk) bonds (5.2eV); similarly, edge bonds have a tendency to be shorter than bulk ones. As a consequence, the flake's interior undergoes a surface induced compression which is the more pronounced the smaller the flake is. This compression manifests itself in the way in which various observables depend on the flake size, N. For example, elastic constants (i.e. Lamé parameters) of small flakes can exceed their bulk limit ($\mu + \lambda \approx 70$eV per ring, $\mu \approx 51$eV per ring, $\nu = 0.162$) by 30% ($\mu + \lambda$) or even by 70% (μ). In comparison, the sheet (out of plane, buckling) stiffness, $\kappa \approx 1.2$eV, is less sensitive to N. Non-linearities remain weak (less than 10% increase) as long as the ratio of out of plane amplitude and in plane wavelength of buckling is below 5%. To highlight the importance of quantum effects on elasticity we have also calculated the vibrational spectrum of graphene flakes. Quantum corrections affect mostly the sheet stiffness, κ, lowering it significantly, about 26% within our DFT framework.

Finally, based on these results we predict a pronounced shift of the Raman G- and D-peaks with decreasing flake size to higher values. It is a natural consequence of the edge induced flake compression. The associated Grüneisen parameters are $\gamma_{\rm D} \approx 2.6$eV/$\mathring{A}^2$ and $\gamma_{\rm G} = 2.2$eV/$\mathring{A}^2$.

VII. ACKNOWLEDGMENTS

[1] K. S. Novoselov, A. K. Geim, S. V. Morozov, D. Jiang, Y. Zhang, S. V. Dubonos, I. V. Grigorieva, and A. A. Firsov, Science **306**, 666 (2004).

[2] Y. Zhang, Y.-W. Tan, H. L. Stormer, and P. Kim, Nature **438**, 201 (2005).

[3] K. S. Novoselov, E. McCann, S. V. Morozov, V. I. Fal'ko, M. I. Katsnelson, U. Zeitler, D. Jiang, F. Schedin, and A. K. Geim, Nature Phys. **2**, 177 (2006).

[4] A. K. Geim and K. S. Novoselov, Nature Mater. **6**, 183 (2007).

[5] K. S. Novoselov, D. Jiang, F. Schedin, T. J. Booth, V. V. Khotkevich, S. V. Morozov, and A. K. Geim, Proc. Natl. Acad. Sci. **102**, 1045 (2005).

[6] A. H. Castro Neto, F. Guinea, N. M. R. Peres, K. S. Novoselov, and A. K. Geim, Rev. Mod. Phys. **81**, 109 (2009).

[7] K. Nakada, M. Fujita, G. Dresselhaus, and M. S. Dresselhaus, Phys. Rev. B **54**, 17954 (1996).

[8] C. Stampfer, J. Güttinger, S. Hellmüller, F. Molitor, K. Ensslin, and T. Ihn, Phys. Rev. Lett. **102**, 056403 (2009).

[9] M. Fujita, K. Wakabayashi, K. Nakada, and K. Kusakabe, J. Phys. Soc. Jap. **65**, 1920 (1996).

[10] L. Brey and H. A. Fertig, Phys. Rev. B **73**, 235411 (2006).

[11] K. Wakabayashi, M. Sigrist, and M. Fujita, J. Phys. Soc. Jap. **67**, 2089 (1998).

[12] Y.-W. Son, M. L. Cohen, and S. G. Louie, Nature **444**, 347 (2006).

[13] Y.-W. Son, M. L. Cohen, and S. G. Louie, Phys. Rev. Lett. **97**, 216803 (2006).

[14] O. Hod, V. Barone, J. E. Peralta, and G. E. Scuseria, Nano Lett. **7**, 2295 (2007).

[15] E. jun Kan, Z. Li, J. Yang, and J. G. Hou, J. Am. Chem. Soc. **130**, 4224 (2008).

[16] N. M. R. Peres, A. H. Castro Neto, and F. Guinea, Phys. Rev. B **73**, 195411 (2006).

[17] L. Pisani, J. A. Chan, B. Montanari, and N. M. Harrison, Phys. Rev. B **75**, 064418 (2007).

[18] D. en Jiang, B. G. Sumpter, and S. Dai, J. Chem. Phys. **127**, 124703 (2007).

[19] J. Fernández-Rossier and J. J. Palacios, Phys. Rev. Lett. **99**, 177204 (2007).

[20] W. L. Wang, O. V. Yazyev, S. Meng, and E. Kaxiras, Phys. Rev. Lett. **102**, 157201 (2009).

[21] C. Gmez-Navarro, M. Burghard, and K. Kern, Nano Lett. **8**, 2045 (2008).

[22] R. Danneau, F. Wu, M. F. Craciun, S. Russo, M. Y. Tomi, J. Salmilehto, A. F. Morpurgo, and P. J. Hakonen, Phys. Rev. Lett. **100**, 196802 (2008).

[23] P. Lauffer, K. V. Emtsev, R. Graupner, T. Seyller, L. Ley, S. A. Reshanov, and H. B. Weber, Phys. Rev. B **77**, 155426 (2008).

[24] X. Li, X. Wang, L. Zhang, Lee, Sangwon, and H. Dai, Science **319**, 1229 (2008).

[25] M. Haluka, D. Obergfell, J. C. Meyer, G. Scalia, G. Ulbricht, B. Krauss, D. H. Chae, T. Lohmann, M. Lebert, M. Kaempgen, et al., Phys. Status Solidi (b) **244**, 4143 (2007).

[26] F. Miao, S. Wijeratne, Y. Zhang, U. C. Coskun, W. Bao, and C. N. Lau, Science **317**, 1530 (2007).

[27] C. Casiraghi, A. Hartschuh, H. Qian, S. Piscanec, C. Georgi, A. Fasoli, K. S. Novoselov, D. M. Basko, and A. C. Ferrari, Nano Lett. **9** (2009).

[28] A. L. V. de Parga, F. Calleja, B. Borca, J. M. C. G. Passeggi, J. J. Hinarejos, F. Guinea, and R. Miranda, Phys. Rev. Lett. **100**, 056807 (2008).

[29] C. L. Tan, Z. B. Tan, K. Wang, L. Ma, F. Yang, F. M. Qu, J. Chen, C. L. Yang, and L. Lu (2009), arXiv/0910.5777.

[30] A. Fasolino, J. H. Los, and M. I. Katsnelson, Nature Materials **6**, 858 (2007).

[31] G. Gui, J. Li, and J. Zhong, Phys. Rev. B **78**, 075435 (2008).

[32] J. Atalaya, A. Isacsson, and J. M. Kinaret, Nano Lett. **8**, 4196 (2008).

[33] D. Garcia-Sanchez, A. M. van der Zande, A. S. Paulo, B. Lassagne, P. L. McEuen, and A. Bachtold, Nano Lett. **8**, 1399 (2008).

[34] C. Lee, X. Wei, J. W. Kysar, and J. Hone, Science **321**, 385 (2008).

[35] V. M. Pereira, A. H. Castro Neto, and N. M. R. Peres, Phys. Rev. B **80**, 045401 (2009).

[36] S.-M. Choi, S.-H. Jhi, and Y.-W. Son, Phys. Rev. B **81**, 081407 (2010).

[37] K. V. Zakharchenko, M. I. Katsnelson, and A. Fasolino, Phys. Rev. Lett. **102**, 046808 (2009).

[38] O. Hod and G. E. Scuseria, Nano Lett. **9**, 2619 (2009).

[39] E. Cadelano, P. L. Palla, S. Giordano, and L. Colombo, Phys. Rev. Lett. **102**, 235502 (2009).

[40] F. Guinea, B. Horovitz, and P. Le Doussal, Solid State Commun **149**, 1140 (2009).

[41] C. D. Reddy, A. Ramasubramaniam, V. B. Shenoy, and Y.-W. Zhang, Appl. Phys. Lett. **94**, 101904 (2009).

[42] Q. Lu, M. Arroyo, and R. Huang, J. Phys. D: Appl. Phys. **42**, 102002 (6pp) (2009).

[43] R. M. Ribeiro, V. M. Pereira, N. M. R. Peres, P. R. Briddon, and A. H. Castro Neto, New J. Phys. **11**, 115002 (2009).

[44] J. C. Meyer, A. K. Geim, M. I. Katsnelson, K. S. Novoselov, T. J. Booth, and S. Roth, **446**, 60 (2007).

[45] E. Stolyarova, K. Rim, S. Ryu, J. Maultzsch, P. Kim, L. Brus, T. Heinz, M. Hybertsen, and G. Flynn, Proc. Natl. Acad. Sci. **104** (2007).

[46] M. Ishigami, J. H. Chen, W. G. Cullen, M. S. Fuhrer, and E. D. Williams, Nano Lett. **7**, 1643 (2007).

[47] W. Bao, F. Miao, Z. Chen, H. Zhang, W. Jang, C. Dames, and C. N. Lau, Nat. Nano. **4**, 562 (2009).

[48] T. M. G. Mohiuddin, A. Lombardo, R. R. Nair, A. Bonetti, G. Savini, R. Jalil, N. Bonini, D. M. Basko, C. Galiotis, N. Marzari, et al., Phys. Rev. B **79**, 205433 (2009).

[49] C. C. Chen, W. Bao, J. Theiss, C. Dames, C. N. Lau, and S. B. Cronin, Nano Lett. (2009).

[50] A. C. Ferrari, J. C. Meyer, V. Scardaci, C. Casiraghi, M. Lazzeri, F. Mauri, S. Piscanec, D. Jiang, K. S. Novoselov, S. Roth, et al., Phys. Rev. Lett. **97**, 187401 (2006).

[51] Z. H. Ni, T. Yu, Y. H. Lu, Y. Y. Wang, Y. P. Feng, and Z. X. Shen, ACS Nano **2**, 2301 (2008).

[52] J. E. Proctor, E. Gregoryanz, K. S. Novoselov, M. Lotya, J. N. Coleman, and M. P. Halsall, Phys. Rev. B **80**, 073408 (2009).

[53] G. Tsoukleri, J. Parthenios, K. Papagelis, R. Jalil, A. C. Ferrari, A. K. Geim, K. S. Novoselov, and C. Galiotis, Small **5**, 2397 (2009).

[54] S. Reich, H. Jantoljak, and C. Thomsen, Phys. Rev. B **61**, R13389 (2000).

[55] D. Sánchez-Portal, E. Artacho, J. M. Soler, A. Rubio, and P. Ordejón, Phys. Rev. B **59**, 12678 (1999).

[56] S. Reich, C. Thomsen, and P. Ordejón, Phys. Rev. B **65**, 153407 (2002).

[57] O. Hod, J. E. Peralta, and G. E. Scuseria, Phys. Rev. B **76**, 233401 (2007).

[58] L. Landau and E. Lifshitz, *Theory of Elasticity, Vol 7* (Pergamon Press, 1959).

[59] R. Ahlrichs, M. Bär, M. Häser, H. Horn, and C. Kölmel, Chem. Phys. Lett. **162**, 165 (1989).

[60] A. D. Becke, Phys. Rev. A **38**, 3098 (1988).

[61] J. P. Perdew, Phys. Rev. B **33**, 8822 (1986).

[62] J. P. Perdew and Y. Wang, Phys. Rev. B **45**, 13244 (1992).

[63] J. P. Perdew, K. Burke, and M. Ernzerhof, Phys. Rev. Lett. **77**, 3865 (1996).

[64] A. D. Becke, J Chem. Phys. **98**, 5648 (1993).

[65] A. Schäfer, H. Horn, and R. Ahlrichs, J Chem. Phys. **97**, 2571 (1992).

[66] N. Mounet and N. Marzari, Phys. Rev. B **71**, 205214 (2005).

[67] K. N. Kudin, G. E. Scuseria, and B. I. Yakobson, Phys. Rev. B **64**, 235406 (2001).

[68] M. Arroyo and T. Belytschko, Phys. Rev. B **69**, 115415 (2004).

[69] R. C. Weast and M. J. Astle, *CRC Handbook of Chemistry and Physics* (CRC press, New York, 2009), 89th ed.

[70] O. L. Blakslee, D. G. Proctor, E. J. Seldin, G. B. Spence, and T. Weng, J. Appl. Phys. **41**, 3373 (1970).

[71] A. Bosak, M. Krisch, M. Mohr, J. Maultzsch, and C. Thomsen, Phys. Rev. B **75**, 153408 (2007).

[72] G. M. Odegard, T. S. Gates, L. M. Nicholson, and K. E. Wise, Compos. Sci. Technol. **62**, 1869 (2002).

[73] P. Deglmann, F. Furche, and R. Ahlrichs, Chem. Phys. Lett. **362**, 511 (2002).

[74] P. Deglmann and F. Furche, J. Chem. Phys. **117**, 9535 (2002).

[75] C. Thomsen, S. Reich, and P. Ordejón, Phys. Rev. B **65**, 073403 (2002).

[76] Note, that certain effects related to the thickness of the graphene sheet are left out in Eq. (2). For example, a linear displacement field ($h(\mathbf{r})=x$, $\mathbf{u}=0$) has no energy cost, because the description assumes, that such a conformation is equivalent to a rotation. However, this ignores that a rotation gives the π_z orbitals a new direction in space, while the lifting up of atoms mediated by the linear displacement field does not. In the latter case, there is an additional energy cost $\propto |\nabla h|^2$ related to the fact, that the overlap of π_z-orbitals changes, which is not included in Eq. (2). Similarly, global rotational invariance is given only for free flakes. It can be broken due to experimental boundary conditions, e.g. the attachment of contacts. Also this may produce gradient terms $(\nabla h)^2$ in the functional (2).

[77] The motion of edge atoms in the plane is further restricted in the sense that only conformations have been considered, which can be obtained by a homogenous rescaling of all C-C edge bond lengths.

[78] Recall that due to the presence of edge the symmetry group of our sample is lower (D_{2h}) than the one of the unperturbed hexagonal unit cell (D_{6h}).

[79] This relaxation process is the limiting computational step. For a flake with $N = 6$ it took several days on a single Opteron processor. For $N=6$ a single iteration takes about 1 day and for full convergence one needs typically 50 days.